https://doi.org/10.5194/essd-2026-95
Preprint. Discussion started: 27 April 2026

Open Access Earth System Science Data Discussions

Dataset of aerosol, ozone, and meteorology observations at the surface coastal site of Henties Bay in Namibia

Paola Formenti[1$], Danitza Klopper[2,*], Anais Feron[1,**], Mathieu Cazaunau[1], Servanne Chevaillier[1], Karine Desboeufs[1], Claudia Di Biagio[1], Clarissa Baldo[1], Cécile Gaimoz[3,***], Vincent Michoud[1], Cécile Mirande-Bret[1,****], Sylvain Triquet[1], François Hemeret[1], Richard Valorso[3], Stephen Broccardo[2,*****], Andreas Namwoonde[4], Mattheus Hanghome[4,******], Chiara Giorio[5], and Stuart J. Piketh[2]

[1] Université Paris Cité and Univ. Paris Est Créteil, CNRS, LISA, F−75013 Paris, France
[2] NorthWest University, Potchefstroom, South Africa
[3] Univ Paris Est Creteil and Université Paris Cité, CNRS, LISA, F−94010 Créteil, France
[4] Sam Nujoma Marine and Coastal Resources Research Centre, University of Namibia, Henties Bay, Namibia
[5] Yusuf Hamied Department of Chemistry, University of Cambridge, Lensfield Road, Cambridge, CB2 1EW, United Kingdom

[*] now at University of Limpopo, Mankweng, South Africa
[**] now at Eco&Phy Saclay, INRAE, France
[***] now at CNRS INSU Division Technique, Gif-Sur-Yvette, France
[****] now at University of Bordeaux, CNRS, Laboratoire de Biogenèse Membranaire (LBM), UMR 5200, F-33140, Villenave d'Ornon, France,
[*****] now at Bay Area Environmental Research Institute / NASA Ames Research Center, Moffett Field, CA, U.S.A.
[******] now at School of Veterinary Medicine, Faculty of Health Sciences and Veterinary Medicine, Department of Preclinical Studies, Neudam Campus, University of Namibia.

[$] Correspondence to: paola.formenti@lisa.ipsl.fr

Abstract

Between 2012 and 2019, measurements of aerosol mass concentration, composition of the inorganic fraction, optical properties, meteorology and ozone were conducted at the Henties Bay Aerosol Observatory (HBAO) located at the Sam Nujoma Marine and Coastal Resources Research Centre of the University of Namibia at Henties Bay (22.09° S, 14.26° E; 30 m above mean sea level) in Namibia. The site aimed at filling a gap in observation of the boundary layer aerosol at the coastal interface between the hyper-arid Namib desert and the south East Atlantic Ocean, characterised by haziness due to frequent mineral dust plumes and persistent sea spray. Some of the data were already validated and analysed by Formenti et al. (2018), Klopper et al. (2020), Desboeufs et al. (2024).

In this paper we present the entire quality-controlled dataset which is now made available to the public with the following DOI:

- Aerosol elemental and water-soluble ionic composition during 2016 (https://doi.org/10.57932/534b9e4e-aa4a-45f3-a538-3faf57168287; Formenti et al., 2026)
- Aerosol elemental, water-soluble ionic and dissolved elemental composition during 2017 (https://doi.org/10.57932/2ac79cd1-282a-4004-87d5-38f0ebcaf40c; Formenti, 2023)
- Aerosol mass concentration between 2012 and 2019 (https://doi.org/10.57932/d5bcf2ef-1c1f-4f87-9945-e5ec9a948112; Valorso et al., 2026a)

https://doi.org/10.5194/essd-2026-95
Preprint. Discussion started: 27 April 2026

- Ozone mixing ratio between 2012 and 2019 (https://doi.org/10.57932/59ed8db1-2a18-4429-a153-fffa61cdbb41; Valorso et al., 2026b)
- Aerosol particle scattering between 2015 and 2019 (https://doi.org/10.57932/4d3613b6-4c49-417f-ac1d-fd825602fbfb; Valorso et al., 2026c)
- Aerosol equivalent black carbon concentration between 2012 and 2019 (https://doi.org/10.57932/c8c755ef-bf7a-441e-a4c6-1ee875e5f570; Valorso et al., 2026d)
- Wind speed and direction between 2012 and 2019 (https://doi.org/10.57932/99b707a5-1cba-4b61-915b-829aa742a726; Valorso et al., 2026e)
- Basic meteorology between 2018 and 2019 (https://doi.org/10.57932/9d344c70-2f09-4fff-a2d9-ce72f5cf1757; Valorso et al., 2026f)

These research-quality data, unique for the area, have many uses, including the determination of seasonal changes in the atmospheric composition and the validation of climate and weather modeling output and satellite-retrieved aerosol products.

1. Introduction

The west coast of southern Africa is a region of great climatic and environmental interest. The region is characterised by many geophysical features, such as the low-level stratocumulus cloud deck, the coastal fog, the oceanic Benguela current, and the hyper-arid Namib desert, promoting strong atmosphere-sea-land exchanges, both in energy and in mass (Andreae et al., 1994; 1995; Louw et al., 2016; Ohde and Dadou, 2018; Spirig et al., 2019 ; Giorio et al., 2022). The west coast of southern Africa is strongly affected by climate change and both the mean surface air temperature and the oceanic water temperatures are predicted to increase by up to 7°C before the end of the current century (Engelbrecht et al., 2015 ; Maure et al., 2018 ; Hoegh-Guldberg et al., 2018 ; Mundy et al., 2025).

Most of the atmospheric research in the area has focused on studying the characteristics, the dynamics and the radiative effetcs of the seasonal biomass burning aerosol smoke plumes from central Africa that give rise to very high optical depth and significant radiative effects while transported at large scale over the region (Swap et al., 2003; Zuidema et al., 2016; Formenti et al., 2019; Redemann et al., 2021; Haywood et al., 2021), and potentially contributing to the changes in the stratus clouds cover over the South Atlantic and the fog lifecycle (Mass et al., 2025; Goessling et al. 2025). On the other hand, little attention has been given to the chemical composition of the boundary layer, notably to aerosol particles, and that despite their potential importance for the cloud and fog formation and the ocean-land biogeochemistry (Andreae et al., 1995; Hegg et al., 2012; Dansie et al., 2018 ; Weston et al., 2022).

Surface continuous atmospheric observations are rare in southern Africa and more generally in the southern hemisphere (Laj et al., 2020; Paton-Walsh et al., 2022; Kanaya et al., 2025). Beside the in situ Global Atmospheric Watch (GAW) station of Cape Point in South Africa (34° 21′S, 18° 29′E; Andrews et al., 2019; hereafter CPT), most of the current knowledge on the long-term variability of the aerosol load on the west coast of southern Africa relies on the

https://doi.org/10.5194/essd-2026-95
Preprint. Discussion started: 27 April 2026

AERONET/PHOTONS distributed network of column sunphotometers (Eck et al., 2003; Holben et al., 2018).

To fill this gap, between 2012 and 2019 the Laboratoire Interuniversitaire des Systèmes Atmosphériques (LISA) in Créteil (France) and the Climatology Research Group (CRG) in Potchefstroom (South Africa) conducted new surface in situ measurements at the Henties Bay Aerosol Observatory (HBAO) at the Sam Nujoma Marine and Coastal Resources Research Centre of the University of Namibia (SANUMARC) at Henties Bay in Namibia. Measurements aimed to describe the temporal variability of the aerosol loads, attribute their sources and characterise some fundamental properties such as composition, light-scattering and absorption. These measurements were complemented by observations of the surface meteorology, ozone concentrations and by a column sun-photometer as part of AERONET/PHOTONS.

The station observations were instrumental in providing new insights on the seasonal variability of the aerosol optical properties and long-range transport of light-absorbing aerosols (Formenti et al., 2018), the source apportionment of the inorganic aerosol composition (Klopper et al., 2020), and the effect of marine emissions on the solubility of dust aerosols (Desboeufs et al., 2024).

As a way forward, the objective of this paper is to describe the entire dataset of observations, which is now available on the Earth System Data Repository (EaSy Data) open portal (https://www.easydata.earth; last accessed 4 february 2026) of the French National research infrastructure Data Terra.

Although it contains discontinuities due to the difficulty in maintaining the instrumentation in a functional state in this challenging environment, the dataset is unique to date, and we expect it to be useful for more process and model validation studies, given the importance of the geographical area in climate and atmospheric chemistry research.

2. Methods

The town of Henties Bay in the Erongo province of Namibia (22.09° S, 14.26° E; 30 m above mean sea level) is located in a coastal arid environment with little to no vegetation. Henties Bay has approximately 5000 inhabitants and little commercial activity, but faces the Cape of Good Hope sea route of commercial shipping from Walvis Bay (approximately 100 km to the south), one of the largest harbours in the Southeast Atlantic Ocean (Namport, 2018).

The geographical position of Henties Bay with respect to the location of some active stations of the AERONET/PHOTONS sunphotometer network is shown in Fig. 1.

https://doi.org/10.5194/essd-2026-95
Preprint. Discussion started: 27 April 2026

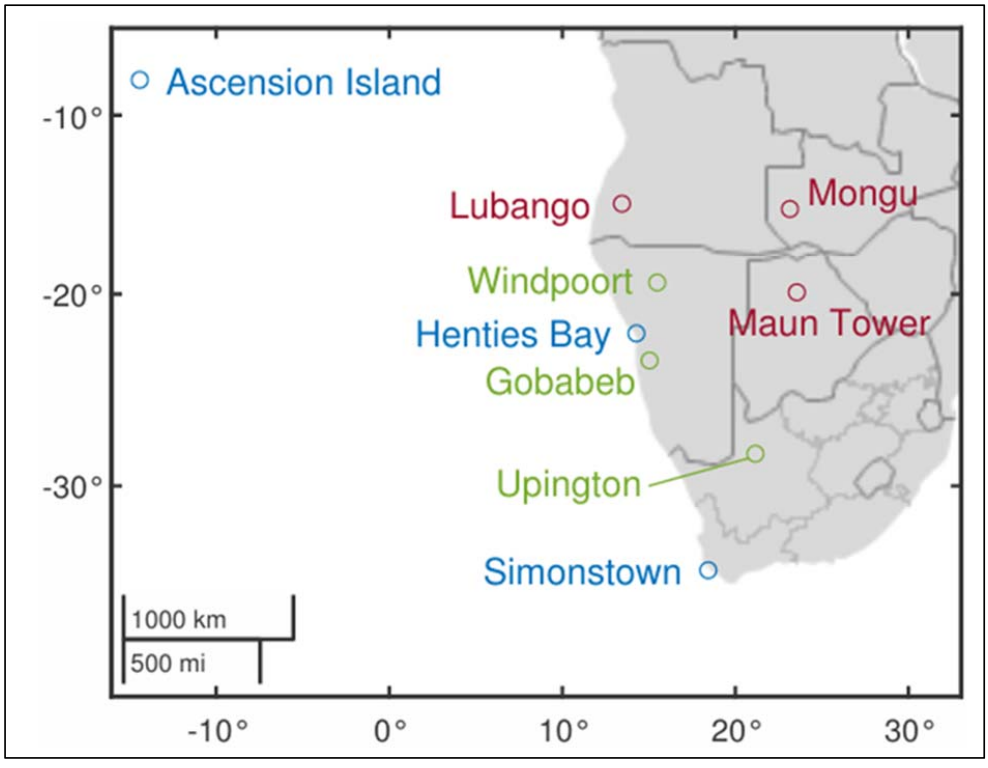

Figure 1. Geographical location of Henties Bay with respect to that of active sunphotometer stations of the regional AERONET/PHOTONS network. Stations at the proximity of wildfire areas are indicated in red. Continental stations are indicated in green. Marine stations are indicated in blue.

The HBAO station is situated on one of the buildings of the SANUMARC campus, approximately 6 km north-west of Henties Bay (Fig. 2). The station consisted of a rooftop terrace approximately 30 m above the ground and 100 m from the shoreline, where sampling inlets were located. These inlets were connected by straight stainless-steel pipes to instruments situated in a room underneath.

https://doi.org/10.5194/essd-2026-95
Preprint. Discussion started: 27 April 2026

Open Access Earth System Science Data Discussions

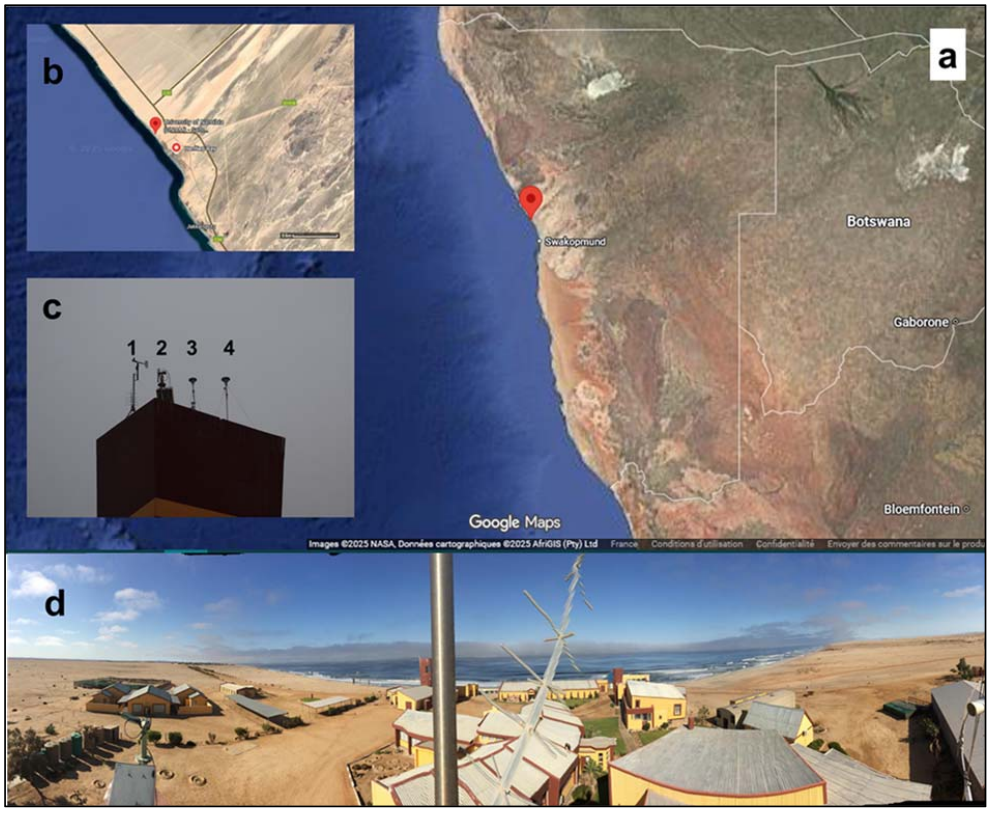

Figure 2. Composite of (a) © Google map showing the location of Henties Bay in Namibia, southern Africa; (b) the location of the University of Namibia campus where HBAO was located on the north-west of the town of Henties Bay; (c) some of the sensors and sampling head on the top of the HBAO tower, that is (1) wind sensor; (2) AERONET/Photons sun/sky photometer (3) PM_{10} sampling head serving the TEOM and nephelometer instruments; (4) PM_{10} sampling head serving the PARTISOL sampler. The PM_1 sampling head serving the aethalometer and the Teflon line serving the ozone analyser are not visible; (d) the view from the top of the HBAO tower to the west, showing the small and few buildings of the University campus and the proximity with the sea shore at approximately than 100 m. The stratocumulus cloud deck is visible at the horizon. Copyright statement: Map data © NASA © 2025 Google.

2.1. Instruments, data acquisition and curation

The operational details of the instrumentation of HBAO are listed in Table 1.

Table 1. Summary of observables and instruments at HBAO.

Observable	Instrument	Operation and time resolution	Period
Particle mass concentrations M_c (PM2.5 fraction until mid-july 2014 and PM_{10} afterwards)	TEOM microbalance (Thermo Inc. model 1405)	Continuous, 5-min	2012-2019
Particle scattering coefficient $_{sca}$ (450, 550, 700 nm, PM_{10} fraction)	Nephelometer (TSI Inc. model 3563)	Continuous, 5-min	2015-2019
Particle absorption coefficient (880 nm, PM_1 fraction)	Aethalometer (Magee Sci. model AE-14U)	Continuous, 5-min	2012-2019
Aerosol elemental composition (PM_{10} fraction)	Partisol (Thermo Inc model 2205)	Twice a day	2016-2017
Ozone mixing ratio	Environmental SA	Continuous, 5-min	2012-2017

https://doi.org/10.5194/essd-2026-95
Preprint. Discussion started: 27 April 2026

	Chemi-luminescence (Environmental SA model O342M Horiba Inc model APOA)		2017-2019
Wind speed and direction	Campbell Scientific 05103 Vaisala WXT530	Continuous, 5-min	2012-2017 2018-2019
Temperature, humidity, pressure	Vaisala weather station	Continuous, 1-min	2018-2019
Column optical properties	CIMEL 318 sunphotometer	Continuous, 1-min	2012-2019

The instrumentation was monitored by on-site personnel and people from LISA and CRG during occasional visits (approximately once per year), and regular checks via remote connection (TeamViewer® version 11) to the computers used for acquisition. All data were acquired and stored on a data logger (model CR-1000, Campbell Sci. Ltd.), except those of the Partisol sampler and the nephelometer, which used their proprietary acquisition software. The team faced the challenges of a marine and moist environment, requiring careful and frequent cleaning of the pipelines, sampling heads, and sensors. This explains why the operating period reported in Table 1 differs significantly from one instrument to another. Some data losses were due to power outages and occasional flooding. The details of the instruments and the respective data curation are described in the following paragraphs.

2.1. Particle mass concentration

The particle mass concentration was measured with a Tapered Element Oscillating Microbalance (TEOM, model 1400a, Rupprecht and Patashnick, Albany, New York, USA). Between 2012 and 2014, the instrument was operated from a certified inlet (also from Rupprecht and Patashnick) to select particles of diameter smaller than 2.5 µm in equivalent aerodynamic diameter ($PM_{2.5}$). After 2014, and until 2019, the inlet was replaced to sample particles of diameter smaller than 10 µm in equivalent aerodynamic diameter (PM_{10}, Rupprecht and Patashnick, Albany, New York, USA). The total flow rate at the inlet was 16.7 L min^{-1}, and the sampling flow rate driving the aerosol-laden air to the microbalance was 3 L min^{-1}. The temperature of the sample stream was kept constant at 50ºC. The instrument has a nominal detection limit of 5 µg m^{-3} and an accuracy of 1 µg m^{-3}. Data were acquired and stored as 5-minute averages. During the acquisition, the instrument flags occurrences of invalid data based on the stability of the temperatures and flow rates. Additionally, the observation record was manually inspected to discard spurious and outlier data (peaks of short duration when concentrations exceeded 200 µg m^{-3}).

2.2. Particle elemental and water-soluble composition

The measurements of the particle elemental and water-soluble composition from the collection of filter samples were already detailed by Klopper et al. (2020) and Desboeufs et al. (2024). During 2016 and 2017, 385 samples were collected on Whatman Nucleopore polycarbonate filters (47-mm diameter, 1-µm pore size) using an automated sequential air sampler (model

https://doi.org/10.5194/essd-2026-95
Preprint. Discussion started: 27 April 2026

Partisol Plus 2025i, Thermo Fisher Scientific, Waltham, MA USA). The instrument operated at 16.7 L min^{-1} (1 m^3 h^{-1}) through a certified PM_{10} inlet (Rupprecht and Patashnick, Albany, New York, USA). The sampling routine consisted of two exposures per day, the first from 09:00 to 18:00 UTC and the second from 21:00 to 06:00 UTC, approximately on an intermittent week-on/week-off schedule. One blank sample per week was collected. All samples were analysed to yield:

1/ the inorganic elemental mass concentration of 24 elements (Na, Mg, Al, Si, P, S, Cl, K, Ca, Ti, V, Cr, Mn, Fe, Co, Ni, Cu, Zn, As, Sr, Pb, Nd, Cd, Ba) by wavelength-dispersive X-ray fluorescence (WD-XRF) using a PW-2404 spectrometer (Panalytical, Almelo, Netherlands) ;

2/ the water-soluble ionic atmospheric concentrations of 16 water-soluble ions (F^-, propionate, formate, acetate, methanesulfonic acid (MSA), Cl^-, Br^-, NO_3-, PO_4^{3-}, SO_4^{2-}, oxalate, Na^+, NH_4^+, K^+, Ca^{2+} and Mg^{2+}) measured by ion chromatography (IC) with a Metrohm IC 850 device ;

3/ during 2017 only, the dissolved atmospheric mass concentrations of 25 water-soluble metals and metalloids, including Fe, Al, and Si, by inductively coupled plasma-atomic emission spectroscopy (ICP-AES; Spectro ARCOS Ametek®) and high-resolution inductively coupled plasma-mass spectrometry (HR-ICP-MS, Neptune Plus™, Thermo Scientific™).

For each chemical species, the minimum quantification limit (MQL) was calculated as 10 times the square root of the standard deviation of the concentration measured on the laboratory blank samples, prepared as actual samples but stored and analysed without exposure to external air. All concentrations above the MQL were corrected for their corresponding average blank value and reported as such in the datasets. The remaining instances are indicated as “MQL”. The MQL values (expressed as concentration per unit filter area or concentration per solution volume) are reported in Klopper et al. (2020).

2.3. Particle equivalent black carbon concentration

The measurements of the particle equivalent black carbon concentration (eBC) in the PM_1 fraction were analysed in Formenti et al. (2018). They are derived from the optical attenuation of light (ATN) measured by a single-wavelength aethalometer (model AE-14U, Magee Sci., Berkeley, CA; Hansen et al., 1984) operating at 880 nm and sampling at 3.5 (± 0.1) L min^{-1} from a certified inlet (BGI Inc., Waltham, MA). The airflow temperature and relative humidity were ambient. Measurements were performed at a 5-min time resolution. The original data set was screened to eliminate spikes and peaks lasting less than two hours, generally associated with occasional nearby open fires for barbequing meat.

https://doi.org/10.5194/essd-2026-95
Preprint. Discussion started: 27 April 2026

The operational equations linking the measured attenuation (ATN) at 880 nm to the eBC is

$$eBC = \frac{1}{MAE_{BC}}\left(\frac{1}{C \cdot R(ATN)}\right)\left(\frac{A}{V}\frac{\Delta ATN}{\Delta t}\right) \quad (1)$$

where A represents the area of the aerosol deposit on the filter, V the volumetric flow rate, and ΔATN/Δt is the variation rate of attenuation with time. The correction factors for multiple scattering (C) and shadowing effect (R(ATN)) were fixed to 3.44 (± 0.21) and 0.93, based on Collaud-Coen et al. (2010) and Weingartner et al. (2003). The mass absorption efficiency for eBC (MAE_{BC}) is prescribed and set to 9.0 (± 1.5) $m^2\ g^{-1}$.

2.4. Particle scattering coefficient

Between April 2015 to June 2019, the aerosol scattering coefficient (σ_{sca}) between 7° and 170° and at 450, 550, and 700 nm was measured by a three-wavelength integrating nephelometer (TSI Inc., model 3563, 5-min resolution) sampling at 13.67 L min^{-1} from the certified PM_{10} inlet of the TEOM (sampling from the auxiliary line). The instrument also measured the particle backscattering coefficient between 90° and 170° thanks to a rotating shutter which was found to be malfunctioning and was shut down in March 2018. While the airflow temperature and relative humidity (RH) were ambient, the RH inside the sensing volume was always reduced to less than 60% due to heat from illumination, so that the measured scattering coefficients can be considered as referring to dry air conditions. The particle scattering and backscattering coefficients (units of Mm^{-1} = 10^{-6} m^{-1}) reported in the level-2 were not corrected for angular truncation (Anderson and Ogren, 1998).

The particle scattering Ångström exponent (SAE) calculated between 450 and 700 nm as

$$SAE = -log\ log\left(\frac{\left(\frac{\sigma_{sca,450\ nm}}{\sigma_{sca,700\ nm}}\right)}{\left(\frac{450}{700}\right)}\right) \quad (2)$$

is also reported in the dataset and can be used to evaluate the dominant aerosol type, and so, indirectly as it provides an indication of particle size, the magnitude of the correction. The air pressure, relative humidity and temperature in the measurement volume are provided, as well as the air temperature measured at the inlet. These measurements allow calculation of standard temperature and pressure conditions for data normalisation.

https://doi.org/10.5194/essd-2026-95
Preprint. Discussion started: 27 April 2026

The nephelometer was calibrated using zero-air and CO_2 as reference gases prior to being sent in the field, but not in the field due to the difficulties in bringing and conserving the gas bottles on top of the building. As a quality-control check, regular zeroing was performed to monitor the extent by which the measurement cavity could be affected by particle deposition and accumulation of dirt. Both the stability and the noise of the zero signal were monitored for this purpose. Data records for which the scattering coefficient at 550 nm was lower than 5 Mm^{-1} or higher than 200 Mm^{-1} for short durations (less than two hours) were discarded from further data analysis.

2.5. Ozone mixing ratio

From July 2012 to September 2017, the ozone mixing ratio (units ppb) was measured by a O342M monitor (Environment S.A., France), which was replaced from September 2017 until March 2019 by a APOA-370 analyser (HORIBA, Japan). Both instruments monitor atmospheric ozone concentrations using a cross flow modulated ultraviolet absorption method, with a detection limit of the order of 0.5 ppb, and an accuracy of the order of 1 ppb. The instruments operated at approximately 0.7 L min^{-1} through a Teflon tube (outside diameter 6 mm) using an internal pump. Data were acquired at a 5-minute time resolution. The data curation of this data stream was extremely delicate, notably because ozone is soluble at air relative humidities above 50% (Seinfeld and Pandis, 2006), which is typical of Henties Bay (see section 3). Concentrations were inspected manually to eliminate excessive noise and erratic events.

2.6. Local meteorology

Local wind speed and direction were measured by a Campbell Scientific 05103 anemometer, replaced with a Vaisala WXT530 from September 2017 onwards. From January 2018, additional sensors were added to measure the air temperature, relative humidity and pressure. Measurements were acquired as 5-min averages. Compared to the previous data records, the curation of the meteorological observations was rather simple as sensors are robust and did not suffer from the conditions of the site that complicated data curation for other instruments in the marine coastal environment.

2.7. Column optical depth

A sun-sky photometer (model 318, CIMEL Electronique, France), part of the AERONET/PHOTONS network, was located on the roof of the station. The instrument was installed in November 2011, preceding the main operations at the station. A few data points are also available for May 2024, in correspondence with a new field campaign. Overall, the data coverage was limited due to the persistence of clouds and fog, as well as several

https://doi.org/10.5194/essd-2026-95
Preprint. Discussion started: 27 April 2026

instrumental problems, notably the mobility of the optical head caused by salt, dust and humidity.

3. Results and discussion

Table 2 reports the basic statistics for the observables measured at HBAO during the respective operating periods. Values for the aerosol mass concentration refer to the period 2014-2019 only as in 2012-2014 the instrument was operated with a $PM_{2.5}$ instead of a PM_{10} inlet.

Table 2. Period mean and standard deviations for the observables discussed in this paper. The minimum and maximum values are reported in brackets.

Properties	Basic statistics
Aerosol mass concentration (µg m^{-3})	41 ± 33 (5-198)
Particle eBC concentration (ng m^{-3})	58 ± 57 (5-390)
Particle scattering coefficient at 550 nm (Mm^{-1})	30 ± 20 (5-198)
Scattering Angstrom Exponent (SAE)	0.6 ± 0.5 (0-2.9)
Ozone (ppb)	20 ± 7 (2-101)
Air temperature (°C)	15.5 ± 2.8(4.8-23)
Air relative humidity (%)	80 ± 12 (8-93)
Air pressure (hPa)	1010 ± 3 (1003-1021)
Wind speed (m s^{-1})	2.8 ± 2.6 (< 22.1)
Wind direction (degrees)	153 ± 108
Aerosol optical depth at 440 nm	0.15 ± 0.13 (0.01 - 1.65)

3.1. Columnar aerosol properties

The time series of the monthly average of the aerosol optical depth (AOD) at 440 nm and the Angstrom exponent (AE) between 440 nm and 870 nm at Henties Bay and some of the sunphotometers of the regional AERONET/PHOTONS network (Fig. 1) are shown in Fig. 3. The respective operating periods are reported in Table S1 in the supplementary material.

https://doi.org/10.5194/essd-2026-95
Preprint. Discussion started: 27 April 2026

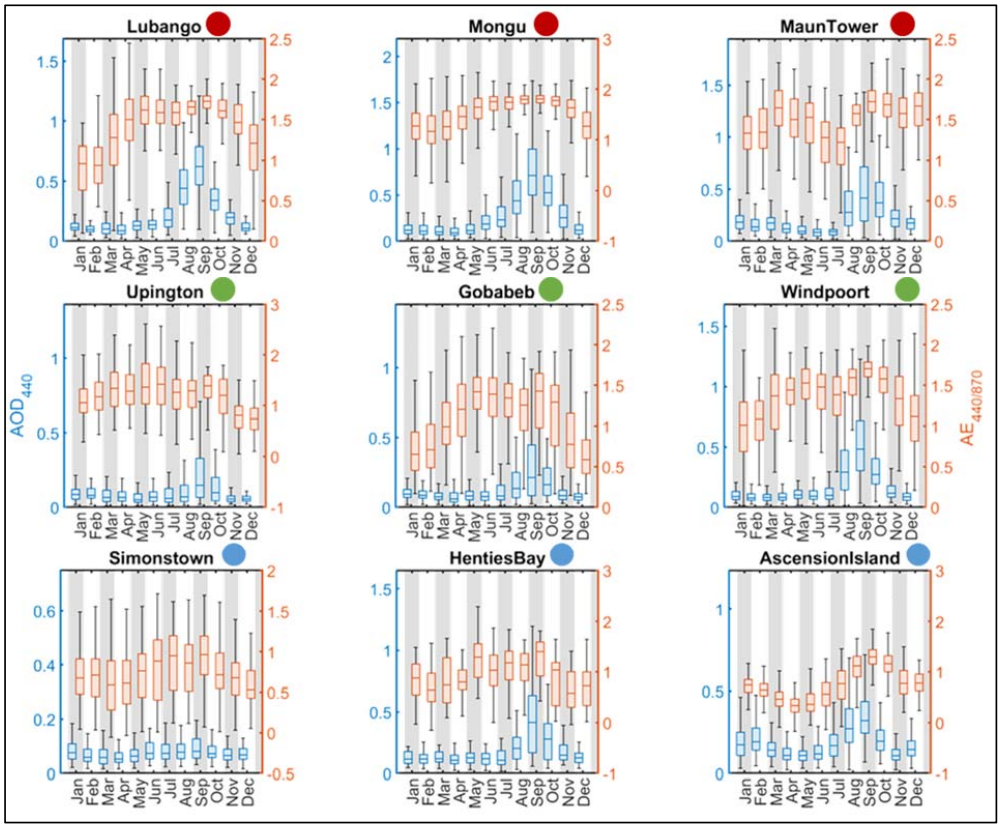

Figure 3. Time series of the monthly average of the aerosol optical depth (AOD) at 440 m (blue boxes, left axis) and the Angstrom exponent between 440 nm and 870 nm (orange boxes, right axes) at Henties Bay and some of the sunphotometers of the regional AERONET/PHOTONS network. The dot next to the station name recalls the color code of Figure 1. Stations at the proximity of wildfire areas are indicated in red. Continental stations are indicated in green. Marine stations are indicated in blue.

The AOD at Henties Bay is characterised by very low to moderate values (averages between 0.08 and 0.4) and a clear seasonal cycle with peak values from August to October. The AOD values are lower than at the sites closer to fire regions (Maun tower, Lubango, Mongu, Windpoort) but similar to values at Ascension Island, Gobabeb and Upington, which all display a very similar seasonal cycle. Differences are evident compared to the coastal station of Simonstown, in South Africa, where AOD is of the order of 0.1 through the year. The average AE is above 1 during August-October, indicating the influence of particles in the accumulation submicron mode, overall suggesting that Henties Bay is affected by the large-scale seasonal transport of biomass burning aerosols occurring in the dry season. The intra-monthly variability is large, indicating the influence of coarse particles, as expected because of the coastal arid

https://doi.org/10.5194/essd-2026-95
Preprint. Discussion started: 27 April 2026

environment of Henties Bay. The monthly values of the column single scattering albedo (SSA) at 440 and 870 nm and the fine and coarse volume fractions are shown in Fig. 4

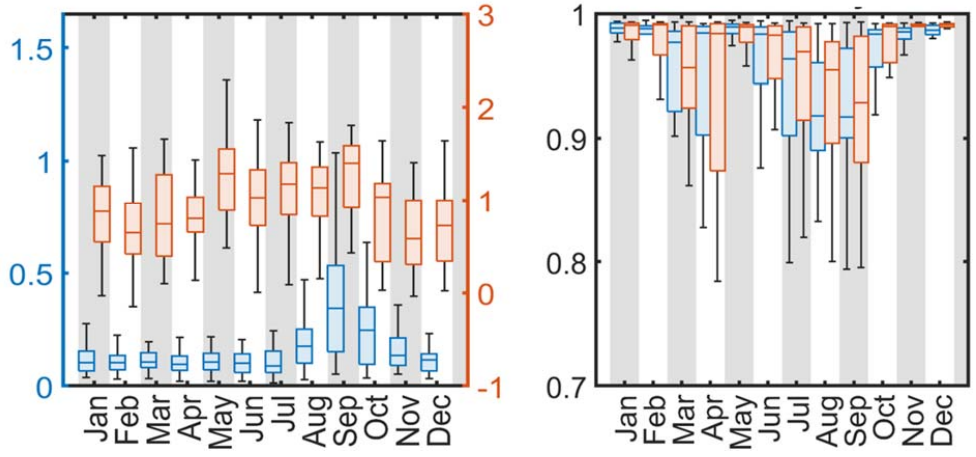

Figure 4. Left panel: Time series of the monthly averages of the column single scattering albedo (SSA) at 440 and 870 nm (blue and orange boxes, respectively). Right panel: Time series of the monthly averages of the fine and coarse volume fractions (blue boxes and left axis and orange boxes and right axis, respectively).

The increased AOD corresponds to a decrease of the SSA and an increase of the fine-mode aerosols, which, however, both occur as early as June, ahead of phase with respect to the seasonality of AOD. On the other hand, the SSA decreases significantly also between March and April, albeit with a different spectral dependence than in June-August, and in correspondence with an increase in the volume of the coarse mode particles, which could indicate that dust particles dominate the aerosol columnar load. The coarse mode particle volume remains elevated also during the October to December period, when on the contrary the SSA increases to values very close to unity, indicating the dominance of scattering maritime aerosols as expected from the general circulation pattern illustrated in Formenti et al. (2018).

3.2. Surface properties and concentrations

The diurnal profiles of each variable are shown in Figure S1 in the supplementary material.

3.2.1. Local meteorology

The record of air temperature, relative humidity and air pressure is limited to 2018-2019. Figure 5 represents their seasonal variability.

https://doi.org/10.5194/essd-2026-95
Preprint. Discussion started: 27 April 2026

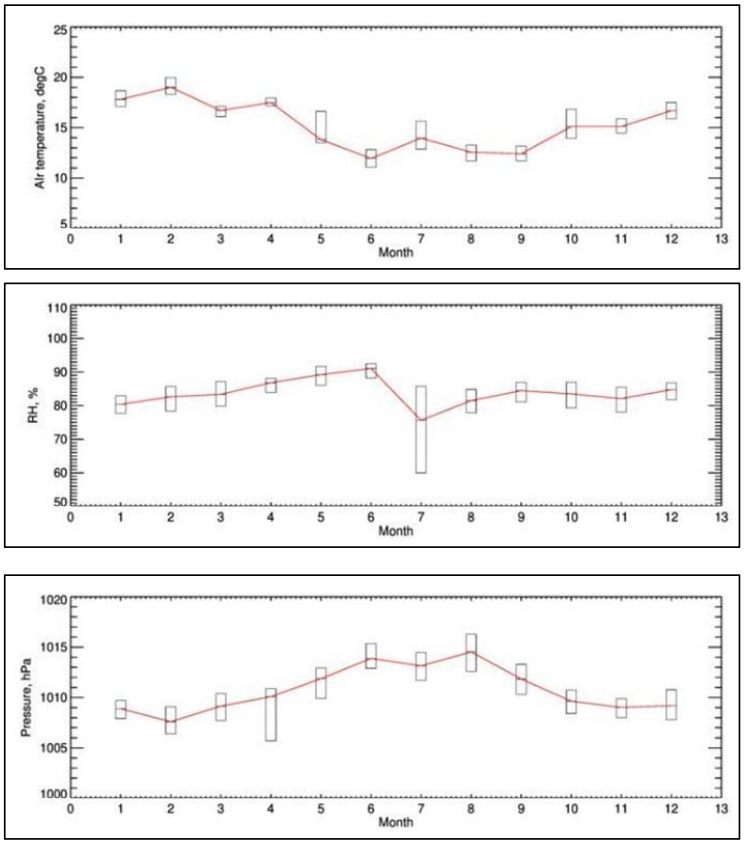

Figure 5. From top to bottom: Air temperature (°C), relative humidity (%) and barometric pressure (hPa). Time series of the monthly 25th and 75th percentiles (black boxes). Median values are indicated by a red line.

Both Table 2 and Fig. 5 show that the atmosphere of Henties Bay was persistently cold and humid over the short temporal extent when measurements were conducted. The median air temperature is of the order of 18°C from October to April, and of the order of 13°C from May to September, in contrast to the barometric pressure which shows the opposite cycle. These meteorological measurements reveal a coastal climate strongly modulated by the semi-permanent South Atlantic Anticyclone (Tyson and Preston-Whyte, 2014). During the austral winter (May–September), this system brings higher atmospheric pressure and cooler temperatures.

The record of wind speed and direction is longer, extending, with interruptions, from 2012 - 2019 (Table 1). These data already informed the analysis of aerosol chemical composition by Klopper et al. (2020), to which we refer for further details. As a complement, Figs. S2 and S3 illustrate the monthly and hourly distributions of these values, respectively. We note here that the mean wind speed is rather low (2.8 ± 2.6 m s^{-1}, Table 2), which is typical for regions

https://doi.org/10.5194/essd-2026-95
Preprint. Discussion started: 27 April 2026

frequently experiencing anti-cyclonic circulation (Klopper et al., 2020). High wind speeds (10-12 m s^{-1}) are generally recorded for southerly winds, which are persistent throughout the year, except in June and July when the highest wind speeds (16-18 m s^{-1}) correspond to north-easterly winds. Both Figs. S1 and S3 show that there is an evident diurnal cycle in the wind speed which peaks between 12h and 16h UTC, regardless of the month of the year. As already noted by Klopper et al. (2020), from May to October, there is also evidence of a sea-land breeze regime where winds tend to be from the continent in the morning to become marine in the early afternoon (Fig S3). Because of the prevalence of southerly to westerly winds, and because the coastline is oriented along the north-to-south-west direction, the local winds at HBAO are henceforth predominantly from the sea.

3.2.2. Total and eBC aerosol mass concentrations

The boundary layer aerosol is a diverse mixture dominated by dust from aeolian erosion and oceanic sea spray and biogenic emissions (Andreae et al., 1995; Vickery et al., 2013; Von Holdt et al., 2019). Despite of the very low population density (Namibia has 3.7 inhabitants per km^2 in 2023; National Census, 2023), the aerosol load is also contributed by anthropogenic emerging commercial activities such as shipping, mining, and energy production (Liebenberg-Enslin et al., 2020; Klopper et al., 2020 ; Formenti et al., 2025).

Fig. 6 shows the monthly variability of the aerosol total and eBC mass concentrations.

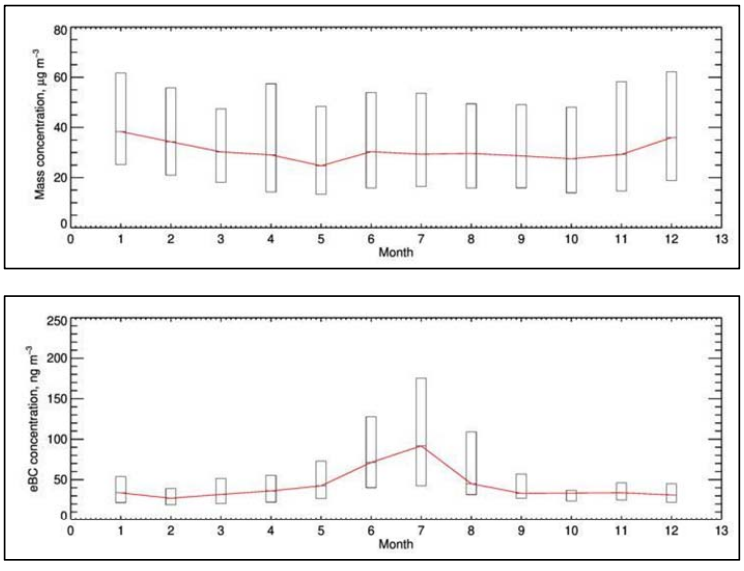

Figure 6. From top to bottom: aerosol mass concentration (µg m^{-3}) and eBC mass concentration (ng m^{-3}). Time series of the monthly 25th and 75th percentiles (black boxes). Median values are indicated by a red line.

https://doi.org/10.5194/essd-2026-95
Preprint. Discussion started: 27 April 2026

The seasonal and diurnal variability of the PM_{10} mass fraction is very limited and the 2014-2019 average reported in Table 2 (41 µg m^{-3}) is close to values measured at coastal sites (e.g., Fomba et al., 2014). However, it is higher than reported for measurements in remote open oceans (e.g., Jiang et al., 2021), likely due to the effect of waves breaking on the sea shore near the sampling site (Zhou et al., 2025). These considerations are consistent with the dominance of south-south westerly winds (Fig. S1, S2 and S3). Indeed, the chemical mass apportionment from filter sampling of Klopper et al. (2020) showed that, regardless of the time of the year, the aerosol load in the PM_{10} mass fraction in the period 2016-2017 was contributed up to approximately 75% by sea salt. On the other hand, a distinct seasonal cycle with hourly concentrations as high as 400 ng m^{-3} is instead observed for eBC (Fig 6 bottom) from May to the end of July, when HBAO is under the anti-cyclonic continental regime (Formenti et al., 2018). Similar values were reported by Andreae et al. (1995) on a cruise transit in the tropical South Atlantic while approaching southern Africa at 19°S. Even at its maximum value, the PM_1 eBC mass represents only a very minor fraction of the PM_{10} mass concentration (0.3% between June and August). From August to late April, the eBC concentrations are similar to those in pristine remote locations including Antarctica (Bodhaine, 1995) or Greenland (von Schneidemesser et al., 2009). As the mass concentration, the eBC displays a negligible diurnal variability (Figure S1).

3.2.3. Metal solubility

The analysis of Klopper et al. (2020) demonstrated that the second largest contributor (up to 20%) to the total PM_{10} aerosol mass was mineral dust. These authors reported 19 episodes during that period 2016-2017, indicating an occasional but frequent transport by both north-easterly and south-to-south-easterly winds. Secondary species (non-sea salt sulphate, MSA, nitrate, fluoride) and heavy metals (notably from mining and heavy-fuel combustion) contributed to about 5%.

HBAO represents an atmospherically interesting environment for investigating multi-phase chemistry in the atmosphere. The site is characterised by frequent fog events, with pH close to neutrality due to the strong marine influence (Giorio et al, 2025). Additionally, the relative humidity often exceeds 80%, while atmospheric aerosols are primarily composed of sea salt (Klopper et al., 2020). Such conditions make the aerosols deliquescent, thereby promoting aqueous-phase chemistry, such as redox cycling and coordination chemistry (Giorio et al., 2025; Formenti et al., 2025). Given the emerging metal-rich anthropogenic influence mixed with strong marine emissions from the coastal part of the Benguela upwelling system, this coastal environment presents a unique opportunity to investigate the processing of aerosols that can influence, for example, iron solubility and therefore nutrient delivery to the nearby ocean (Desboeufs et al., 2024; Formenti et al., 2025) provided with the first estimation of the

https://doi.org/10.5194/essd-2026-95
Preprint. Discussion started: 27 April 2026

iron solubility from natural and anthropogenic dust in the area, and highlighted the role of multi-phase processing by secondary compounds, notably from marine biogenic emissions.

Here, we complete those analyses by reporting additional observations in 2017 of the soluble fraction of several trace metals (Fig. 7).

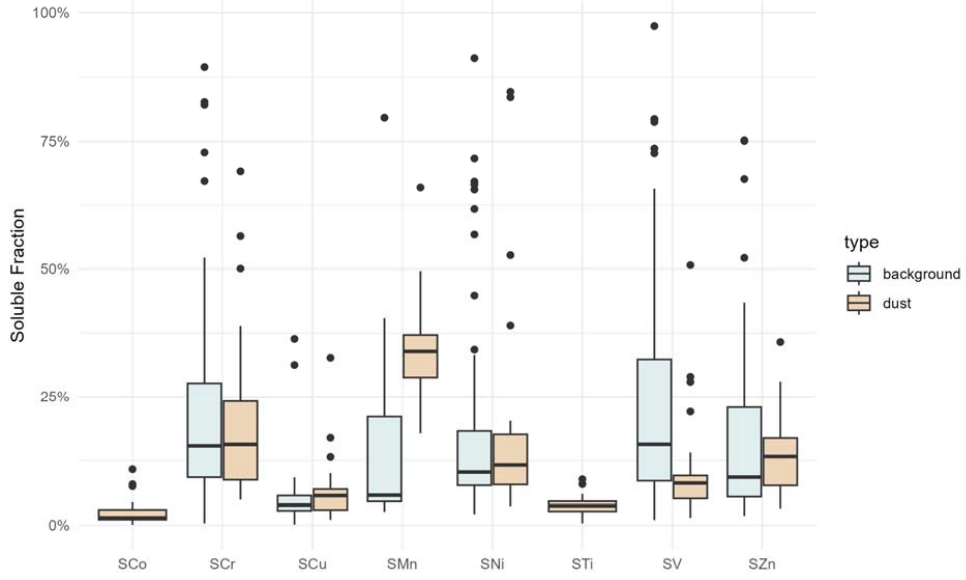

Figure 7. Fractional solubility of trace metals (SX, X = trace metal, expressed in %) measured in the PM_{10} mass fraction. The boxplots indicate the interquartile range, i.e., the 25th and 75th percentiles, and the line within the box marks the median. The whiskers indicate the quartiles ±1.5 times the interquartile range. Points above the whiskers indicate outliers outside the 10th and 90th percentiles. Values for background periods are indicated in blue and values for dust events are indicated in brown. For Co and Ti, only dust-period values are reported as values during background periods were below the MQL.

The distinction of background and dust periods in Fig. 7 follows Desboeufs et al. (2024). A wide range of fractional solubilities of trace elements was observed, with values up to around 100% depending on the element. This appears to be higher than the metal solubility observed in dust source regions, which tends to be below 10% (Baker et al., 2006; Li et al., 2022), but comparable to that of aerosols transported from African air masses over the Atlantic Ocean undergoing atmospheric processing (Shelley et al., 2018). The fractional solubility of Mn and Ti was significantly higher during the dust periods, as was that of Fe (Desboeufs et al., 2024), which is unexpected, as crustal-sourced metals tend to have low solubility unless exposed to low pH conditions and the presence of metal ligands, for example, when mineral dust is mixed with pollutants from various sources (Shi et al., 2012). In this case, the higher fractional solubility during the dust events can be attributed to marine biogenic emissions, as reported for Fe by Desboeufs et al. (2024).

https://doi.org/10.5194/essd-2026-95
Preprint. Discussion started: 27 April 2026

Ni, Cr, Cu, and Zn, which are predominantly sourced from industrial/anthropogenic activities, showed equivalent fractional solubility regardless of time. On the other hand, the fractional solubility of V was significantly higher during the background periods, influenced by fugitive dust from mining activities and heavy-fuel combustion as reported by Klopper et al. (2020).

3.2.4. Aerosol scattering coefficient and mass scattering efficiency

Fig. 8 shows the monthly variability of particle scattering coefficient at 550 nm and SAE.

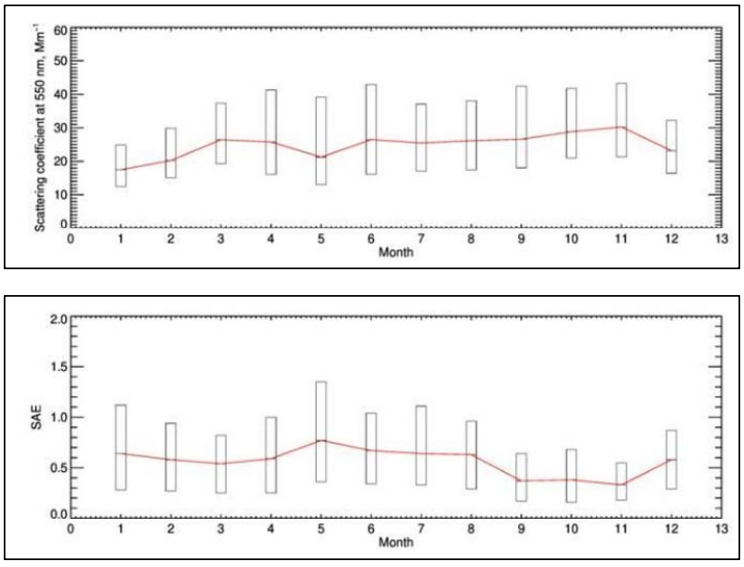

Figure 8. From top to bottom: particle scattering coefficient at 550 nm (Mm^{-1}) and SAE. Time series of the monthly 25th and 75th percentiles (black boxes). Median values are indicated by a red line.

The monthly median values of σ_{scatt} at 550 nm between 18 and 30 Mm^{-1} (Fig. 8) and the low SAE values (mean 0.5 ± 0.6) are in the expected range of measurements at coastal marine locations little influenced by air pollution (e.g., Gassò et al, 2000; Formenti et al., 2001; Pandolfi et al., 2018), consistently with measurements at GAW CPT (Andrews et al., 2019) and Ascension Island (8°S, 14.5°W), 3500 km west of Henties Bay (Zuidema et al., 2018 ; see Figure S4 in the supplementary material). The ratio of σ_{catt} to the total mass concentration yields the PM_{10} mass scattering efficiency (MSE), which at 550 nm ranged from 0.5 (January) to 1 $m^2\ g^{-1}$ (November). This is on the lower side of the average coarse mode sea salt MSE value (1 $m^2\ g^{-1}$) recommended by Hand and Malm (2007), and significantly lower than the average value (1.7 ± 0.9 $m^2\ g^{-1}$) measured by Denjean et al. (2016) in the background marine atmosphere affected by long-range transport of atmospheric pollution. Fig S5 shows that the temporal variability and the magnitude of σ_{catt} at 550 nm can be approximated by a simple multi-linear model as the sum of the contributions of sea salt (MSE = 0.7 $m^2\ g^{-1}$), mineral dust

https://doi.org/10.5194/essd-2026-95
Preprint. Discussion started: 27 April 2026

(MSE = 0.7 m^2 g^{-1}; Hand and Malm, 2007), and non-sea salt sulphate, representing all secondary species (MSE = 8 m^2 g^{-1}; Formenti et al., 2001). Indeed, there is no evidence of the seasonal variability of the eBC concentrations (Fig. 6), confirming that the influence of this low-level transport to the particle scattering is negligible. Fig. S6 additionally shows that the temporal variability of scattering coefficient at the surface and the column AOD had limited to no similarity, as a result of the strong decoupling between the marine boundary layer and the free troposphere (Tyson and Preston-Whyte, 2014).

3.2.6. Ozone

Ozone mixing ratios are in the range of the surface coastal observations in the southern hemisphere, including CPT as reported by Combrink et al. (1995), Lu et al. (2019) and more recently by Kanaya et al. (2025), amongst others. The diurnal cycle is also very weak (Fig S. There is a very moderate but visible seasonal cycle (Fig. 9), with mixing ratios varying from approximately 15 ppb in the austral summertime (December-March) to 20-25 ppb from May to October, when precursors from continental air masses affected by pollution (fuel or biomass burning) are transported at the site.

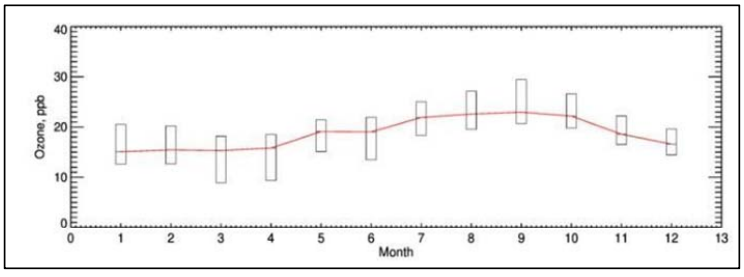

Figure 9. Surface ozone: time series of the monthly 25th and 75th percentiles (black boxes). Median values are indicated by a red line.

The amplitude of the summer minimum and the wintertime maximum at HBAO is similar but smaller to that of CPT (Combrink et al., 1995), and the winter maximum occurs later (September at HBAO while between May and July at CPT). There are many competing processes that could explain the variability (or rather, lack of variability) at both scales, notably the limited insolation and persistence of the inversion layer due to the cloud deck, but also the difference in precursors, as the September peak suggest that the ozone at HBAO could be more related to the surface transport of precursors with biomass burning air masses.

4. Data availability

The dataset of quality-controlled and validated observations (level 2) accessible via the EasyData website is summarised in Table 3. Data are provided in ASCII format as semi-colon-

https://doi.org/10.5194/essd-2026-95
Preprint. Discussion started: 27 April 2026

485 separated files. The in situ online observations are provided at 5-minute time-resolution, with the exception that measurements of elemental and water-soluble fraction are provided at the native 9-hour resolutions. Time stamps are reported in Coordinated Universal Time (UTC). Instances of instrument malfunctioning affecting the data quality are flagged as NA.

Table 3. Name and web reference of the datasets discussed in this paper.

Dataset	URL	References
Namibia_HBAO_elemental_concentrations_2016–v1.txt	https://doi.org/10.57932/534b9e4e-aa4a-45f3-a538-3faf57168287	Formenti et al. (2026)
Namibia_HBAO_elemental_concentrations_2017.txt	https://doi.org/10.57932/2ac79cd1-282a-4004-87d5-38f0ebcaf40c	Formenti (2023)
Namibia_HBAO_water-soluble-ionic_concentrations_2016-v1.txt	https://doi.org/10.57932/534b9e4e-aa4a-45f3-a538-3faf57168287	Formenti et al. (2026)
Namibia_HBAO_water-soluble-ionic_concentrations_2017.txt	https://doi.org/10.57932/2ac79cd1-282a-4004-87d5-38f0ebcaf40c	Formenti (2023)
Namibia_HBAO_dissolved-elemental_concentrations_2017.txt	https://doi.org/10.57932/2ac79cd1-282a-4004-87d5-38f0ebcaf40c	Formenti (2023)
Namibia_HBAO_aerosol_mass_concentration_2012-2019.txt	https://doi.org/10.57932/d5bcf2ef-1c1f-4f87-9945-e5ec9a948112	Valorso et al. (2026a)
Namibia_HBAO_ozone_mixing_ratio_2012-2019.txt	https://doi.org/10.57932/59ed8db1-2a18-4429-a153-fffa61cdbb41	Valorso et al. (2026b)
Namibia_HBAO_aerosol_scattering_2015-2019.txt	https://doi.org/10.57932/4d3613b6-4c49-417f-ac1d-fd825602fbfb	Valorso et al. (2026c)
Namibia_HBAO_eBC_mass_concentration_2012-2019.txt	https://doi.org/10.57932/c8c755ef-bf7a-441e-a4c6-1ee875e5f570	Valorso et al. (2026d)
Namibia_HBAO_wind_speed_direction_2012-2019.txt	https://doi.org/10.57932/99b707a5-1cba-4b61-915b-829aa742a726	Valorso et al. (2026e)
Namibia_HBAO_meteo_2018-2019.txt	https://doi.org/10.57932/9d344c70-2f09-4fff-a2d9-ce72f5cf1757	Valorso et al. (2026f)

490

Data from the AERONET/PHOTONS sunphotometer are available from the AERONET/PHOTONS website (https://aeronet.gsfc.nasa.gov/). The Henties Bay aerosol observatory (HBAO) website is available at http://www.hbao.cnrs.fr/ (last access: 22 September 2025)

495 **5. Conclusions**

Measurements of short-lived species such as aerosols and ozone are rare in the southern hemisphere, and particularly on the west coast of southern Africa, where only the GAW CPT station is active (Andrews et al., 2019; Laj et al., 2020; Patton-Walsh et al., 2022; Kanaya et al., 2025). This limits the knowledge of the fundamental environmental processes and 500 exchanges at the ocean-land-atmosphere interface, contributing to climate change in this vulnerable region of the world.

HBAO is a remote and challenging site. The meteorological record provided by the dataset is critical for interpreting the local atmospheric composition. The dominant south-southwesterly winds and low wind speeds confirm the primacy of marine aerosol sources. The dataset 505 additionally shows that both the local and synoptic meteorology play a significant role, as the seasonal oscillation of temperature and pressure under the influence of the South Atlantic Anticyclone provides the dynamical framework for the wintertime transport of continental

https://doi.org/10.5194/essd-2026-95
Preprint. Discussion started: 27 April 2026

aerosols, notably from biomass burning, to this coastal site Formenti et al. (2018; 2025). The available observations, despite their moderate continuity, are to date unique and they are valuable in representing some of the variables essential to understanding the atmospheric composition on the west coast of southern Africa. The site is presently discontinued for long-term observations, but remains active for intensive field campaigns and fog monitoring (Formenti et al., 2025; Mupambwa et al., 2025).

Author contributions

This dataset was created by RV and PF. AF, MC, CG, SB, AN, MH, DK, SPJ, and PF operated the instrumentation. SC, KD, ST, CMB, and PF performed the XRF, IC and ICP-OES analysis of the collected samples. DK, VM, CB, CG, KD, FH; SJP and PF analysed the results. PF wrote the paper with contributions and comments from all the co-authors. PF and SJP were PIs for HBAO.

Competing interests

CG is a member of the editorial board of Atmospheric Chemistry and Physics. PF is guest editor for the « Aerosol, fog, climate, and biogeochemistry in southern Africa » (ACP/AMT/AR/ESSD inter-journal SI) special issue. The remaining authors have no other competing interests to declare.

Disclaimer

Copernicus Publications remains neutral with regard to jurisdictional claims made in the text, published maps, institutional affiliations, or any other geographical representation in this paper. While Copernicus Publications makes every effort to include appropriate place names, the final responsibility lies with the authors. Views expressed in the text are those of the authors and do not necessarily reflect the views of the publisher.

Special issue statement

This article is part of the « Aerosol, fog, climate, and biogeochemistry in southern Africa » (ACP/AMT/AR/ESSD inter-journal SI) special issue. It is not associated with a conference.

Acknowledgements

The directors of the SANUMARC research centre, Prof. Hilkka Ndjaula, Prof. Edosa Omoregie and Prof. Samuel Mafwila, are sincerely acknowledged for supporting the installation and maintenance of the sampling site through the years. The help of Guillaume Brissebrat (CNRS/DATA TERRA/Aeris), Hélène Bressan, and Sylvain Grellet (GaiaData BRGM) in creating the DOIs for the different datasets and solving the access issues is gratefully

https://doi.org/10.5194/essd-2026-95
Preprint. Discussion started: 27 April 2026

acknowledged. Thanks are due to Marc Daniel Mallet (University of Tasmania) and Tomas Kauna Namupala (SANUMARC) who contributed to the observations and data acquisition.

Financial support

This work has received funding by the French Centre National de la Recherche Scientifique (CNRS) and the South African National Research Foundation (NRF) through the "Groupement de Recherche Internationale Atmospheric Research in southern Africa and the Indian Ocean" (GDRI-ARSAIO) and the Project International de Coopération Scientifique (PICS) "Longterm observations of aerosol properties in Southern Africa" (contract no. 260888) as well as by the Partenariats Hubert Curien (PHC) PROTEA (contract n. 33913SF) funded in France by the French Ministry of Europe and Foreign Affairs (MEAE), supported by the French Ministry of High Education, Research and Innovation (MESRI), and in South Africa by the National Research Foundation. Danitza Klopper is grateful for the financial support of the Climatology Research Group of North-West University and the travel scholarship of the French Embassy in South Africa (internship at LISA in summer 2018).

References

Anderson, T. L., and Ogren, J. A.: Determining aerosols radiative properties using the TSI 3563 integrating nephelometer, Aeros. Sci. Tech., 29, 57-69, 1998.

Andreae, T. W., Andreae, M. O., and Schebeske, G.: Biogenic sulfur emissions and aerosols over the tropical South Atlantic: 1. Dimethylsulfide in sea water and in the atmospheric boundary layer, J. Geophys. Res.,, 99, 22819-22829, https://doi.org/10.1029/94JD01837, 1994.

Andreae, M. O., W. Elbert, and S. J. de Mora, Biogenic sulfur emissions and aerosols over the tropical South Atlantic: Atmospheric dimethylsulfide, aerosols and cloud condensation nuclei. J. Geophys. Res., 100, 11 335–11 356, https://doi.org/10.1029/94JD02828, 1995b.

Andrews, E., Sheridan, P. J., Ogren, J. A., Hageman, D., Jefferson, A., Wendell, J., Alástuey, A., Alados-Arboledas, L., Bergin, M., Ealo, M., Hallar, A. G., Hoffer, A., Kalapov, I., Keywood, M., Kim, J., Kim, S.-W., Kolonjari, F., Labuschagne, C., Lin, N.-H., Macdonald, A., Mayol-Bracero, O. L., McCubbin, I. B., Pandolfi, M., Reisen, F., Sharma, S., Sherman, J. P., Sorribas, M., and Sun, J.: Overview of the NOAA/ESRL Federated Aerosol Network, Bulletin of the American Meteorological Society, 100, 123-135, https://doi.org/10.1175/BAMS-D-17-0175.1, 2019.

Baker, A. R., Jickells, T. D., Witt, M., and Linge, K. L.: Trends in the solubility of iron, aluminium, manganese and phosphorus in aerosol collected over the Atlantic Ocean, Marine Chemistry, 98, 43-58, https://doi.org/10.1016/j.marchem.2005.06.004, 2006.

Bodhaine, B. A., Aerosol absorption measurements at Barrow, Mauna Loa, and South Pole, J. Geophys. Res., 100, 8967–8975, 1995.

Carrico, C. M., Rood, M. J., Ogren, J. A., Neusüß, C., Wiedensohler, A., and Heintzenberg, J.: Aerosol Optical properties at Sagres, Portugal during ACE-2, Tellus B, 52, 694-715, 10.1034/j.1600-0889.2000.00049.x, 2000.

Collaud Coen, M., Weingartner, E., Apituley, A., Ceburnis, D., Fierz-Schmidhauser, R., Flentje, H., Henzing, J. S., Jennings, S. G., Moerman, M., Petzold, A., Schmid, O., and Baltensperger, U.: Minimizing light absorption measurement artifacts of the Aethalometer: evaluation of five correction algorithms, Atmos. Meas. Tech., 3, 457-474, 10.5194/amt-3-457-2010, 2010.

Combrink, J., Diab, R. D., Sokolic, F., and Brunke, E. G.: Relationship between surface, free tropospheric and total column ozone in two contrasting areas in South Africa, Atmospheric Environment, 29, 685-691, https://doi.org/10.1016/1352-2310(94)00313-A, 1995.

https://doi.org/10.5194/essd-2026-95
Preprint. Discussion started: 27 April 2026

Dansie, A. P., Thomas, D. S. G., Wiggs, G. F. S., and Munkittrick, K. R.: Spatial variability of ocean fertilizing nutrients in the dust-emitting ephemeral river catchments of Namibia, Earth Surface Processes and Landforms, 43, 563-578, https://doi.org/10.1002/esp.4207, 2018.

Denjean, C., P. Formenti, K. Desboeufs, S. Chevaillier, S. Triquet, M. Maillé, M. Cazaunau, B. Laurent, O. L. Mayol-Bracero, P. Vallejo, M. Quiñones, I. E. Gutierrez-Molina, F. Cassola, P. Prati, E. Andrews, and J. Ogren, Size distribution and optical properties of African mineral dust after intercontinental transport, J. Geophys. Res. Atmos., 121, 7117–7138, doi:10.1002/2016JD024783, 2016.

Desboeufs, K., Formenti, P., Torres-Sánchez, R., Schepanski, K., Chaboureau, J.-P., Andersen, H., Cermak, J., Feuerstein, S., Laurent, B., Klopper, D., Namwoonde, A., Cazaunau, M., Chevaillier, S., Feron, A., Mirande-Bret, C., Triquet, S., and Piketh, S. J.: Fractional solubility of iron in mineral dust aerosols over coastal Namibia: a link to marine biogenic emissions?, Atmos. Chem. Phys., 24, 1525–1541, https://doi.org/10.5194/acp-24-1525-2024, 2024.

Eck, T. F., Holben, B. N., Ward, D. E., Mukelabai, M. M., Dubovik, O., Smirnov, A., Schafer, J. S., Hsu, N. C., Piketh, S. J., Queface, A., Roux, J. L., Swap, R. J., and Slutsker, I.: Variability of biomass burning aerosol optical characteristics in southern Africa during the SAFARI 2000 dry season campaign and a comparison of single scattering albedo estimates from radiometric measurements, Journal of Geophysical Research: Atmospheres, 108, doi:10.1029/2002JD002321, 2003.

Engelbrecht, F., Adegoke, J., Bopape, M.-J., Naidoo, M., Garland, R., Thatcher, M., McGregor, J., Katzfey, J., Werner, M., Ichoku, C., and Gatebe, C.: Projections of rapidly rising surface temperatures over Africa under low mitigation, Environmental Research Letters, 10, 085004, 10.1088/1748-9326/10/8/085004, 2015.

Fomba, K. W., Müller, K., van Pinxteren, D., Poulain, L., van Pinxteren, M., and Herrmann, H.: Long-term chemical characterization of tropical and marine aerosols at the Cape Verde Atmospheric Observatory (CVAO) from 2007 to 2011, Atmos. Chem. Phys., 14, 8883–8904, https://doi.org/10.5194/acp-14-8883-2014, 2014.

Formenti, P., et al, Aerosol optical properties and large-scale transport of air masses: Observations at a costal and a semiarid site in the eastern Mediterranean during summer 1998, J. Geophys. Res., 106, 9807-9826, 2001.

Formenti, P., Piketh, S. J., Namwoonde, A., Klopper, D., Burger, R., Cazaunau, M., Feron, A., Gaimoz, C., Broccardo, S., Walton, N., Desboeufs, K., Siour, G., Hanghome, M., Mafwila, S., Omoregie, E., Junkermann, W., and Maenhaut, W.: Three years of measurements of light-absorbing aerosols over coastal Namibia: seasonality, origin, and transport, Atmos. Chem. Phys., 18, 17003–17016, https://doi.org/10.5194/acp-18-17003-2018, 2018.

Formenti, P., B. D'Anna, C. Flamant, M. Mallet, S.J. Piketh, K. Schepanski, F. Waquet, F. Auriol, G. Brogniez, F. Burnet, J. Chaboureau, A. Chauvigné, P. Chazette, C. Denjean, K. Desboeufs, J. Doussin, N. Elguindi, S. Feuerstein, M. Gaetani, C. Giorio, D. Klopper, M.D. Mallet, P. Nabat, A. Monod, F. Solmon, A. Namwoonde, C. Chikwililwa, R. Mushi, E.J. Welton, and B. Holben: The Aerosols, Radiation and Clouds in Southern Africa Field Campaign in Namibia: Overview, Illustrative Observations, and Way Forward. Bull. Amer. Meteor. Soc., 100, 1277–1298, https://doi.org/10.1175/BAMS-D-17-0278.1, 2019.

Formenti, P., Atmospheric concentrations of total and dissolved elements and water-soluble ions measured over coastal Namibia in 2017. https://doi.org/10.57932/2ac79cd1-282a-4004-87d5-38f0ebcaf40c, 2023

Formenti, P., Giorio, C., Desboeufs, K., Zherebker, A., Gaetani, M., Baldo, C., Landrot, G., Montebello, S., Chevaillier, S., Triquet, S., Siour, G., Di Biagio, C., Battaglia, F., Doussin, J.-F., Feron, A., Namwoonde, A., and Piketh, S. J.: Elemental composition, iron mineralogy, and solubility of anthropogenic and natural mineral dust aerosols in Namibia: a case study analysis from the AEROCLO-sA campaign – Part 2, Atmos. Chem. Phys., 25, 16127–16145, https://doi.org/10.5194/acp-25-16127-2025, 2025.

Formenti, P., Desboeufs, K., Chevaillier, S., Triquet, S., and S. Piketh, Atmospheric concentrations of total elements and water-soluble ions measured over coastal Namibia in 2016 – v1. https://doi.org/10.57932/534b9e4e-aa4a-45f3-a538-3faf57168287.

https://doi.org/10.5194/essd-2026-95
Preprint. Discussion started: 27 April 2026

Gassó, S., Hegg, D. A., Covert, D. S., Collins, D., Noone, K. J., Öström, E., Schmid, B., Russell, P. B., Livingston, J. M., Durkee, P. A., and Jonsson, H.: Influence of humidity on the aerosol scattering coefficient and its effect on the upwelling radiance during ACE-2, Tellus B, 52, 546-567, 10.1034/j.1600-0889.2000.00055.x, 2000.

Giorio, C., Doussin, J.-F., D'Anna, B., Mas, S., Filippi, D., Denjean, C., Mallet, M. D., Bourrianne, T., Burnet, F., Cazaunau, M., Chikwililwa, C., Desboeufs, K., Feron, A., Michoud, V., Namwoonde, A., Andreae, M. O., Piketh, S. J., and Formenti, P.: Butene emissions from coastal ecosystems may contribute to new particle formation, Geophysical Research Letters, n/a, e2022GL098770, https://doi.org/10.1029/2022GL098770, 2022

Giorio, C., Monod, A., Di Marco, V., Herckes, P., Napolitano, D., Sullivan, A., Landrot, G., Warnes, D., Nasti, M., D'Aronco, S., Gérardin, A., Brun, N., Desboeufs, K., Triquet, S., Chevaillier, S., Di Biagio, C., Battaglia, F., Burnet, F., Piketh, S. J., Namwoonde, A., Doussin, J.-F., and Formenti, P.: Contrasting solubility and speciation of metal ions in total suspended particulate matter and fog from the coast of Namibia – Part 1, Atmos. Chem. Phys., 25, 16107–16125, https://doi.org/10.5194/acp-25-16107-2025, 2025.

Goessling, H. F., Rackow, T., and Jung, T.: Recent global temperature surge intensified by record-low planetary albedo, Science, 387, 68-73, doi:10.1126/science.adq7280, 2025.

Hand, J. L., and Malm, W. C.: Review of aerosol mass scattering efficiencies from ground-based measurements since 1990, J. Geophys. Res., 112, https://doi.org/10.1029/2007JD008484, 2007.

Haywood, J. M., Abel, S. J., Barrett, P. A., Bellouin, N., Blyth, A., Bower, K. N., Brooks, M., Carslaw, K., Che, H., Coe, H., Cotterell, M. I., Crawford, I., Cui, Z., Davies, N., Dingley, B., Field, P., Formenti, P., Gordon, H., de Graaf, M., Herbert, R., Johnson, B., Jones, A. C., Langridge, J. M., Malavelle, F., Partridge, D. G., Peers, F., Redemann, J., Stier, P., Szpek, K., Taylor, J. W., Watson-Parris, D., Wood, R., Wu, H., and Zuidema, P.: The CLoud–Aerosol–Radiation Interaction and Forcing: Year 2017 (CLARIFY-2017) measurement campaign, Atmos. Chem. Phys., 21, 1049–1084, https://doi.org/10.5194/acp-21-1049-2021, 2021.

Hegg, D. A., Covert, D. S., Jonsson, H. H., and Woods, R. K.: A simple relationship between cloud drop number concentration and precursor aerosol concentration for the regions of Earth's large marine stratocumulus decks, Atmos. Chem. Phys., 12, 1229-1238, 10.5194/acp-12-1229-2012, 2012.

Hoegh-Guldberg, O., Poloczanska, E. S., eds. (2018). Effects of Climate Change Across Ocean Regions. Lausanne: Frontiers Media. doi: 10.3389/978-2-88945-502-7

Holben, B. N., Kim, J., Sano, I., Mukai, S., Eck, T. F., Giles, D. M., Schafer, J. S., Sinyuk, A., Slutsker, I., Smirnov, A., Sorokin, M., Anderson, B. E., Che, H., Choi, M., Crawford, J. H., Ferrare, R. A., Garay, M. J., Jeong, U., Kim, M., Kim, W., Knox, N., Li, Z., Lim, H. S., Liu, Y., Maring, H., Nakata, M., Pickering, K. E., Piketh, S., Redemann, J., Reid, J. S., Salinas, S., Seo, S., Tan, F., Tripathi, S. N., Toon, O. B., and Xiao, Q.: An overview of mesoscale aerosol processes, comparisons, and validation studies from DRAGON networks, Atmos. Chem. Phys., 18, 655–671, https://doi.org/10.5194/acp-18-655-2018, 2018.

Kanaya, Y., Sommariva, R., Saiz-Lopez, A., Mazzeo, A., Koenig, T. K., Kawana, K., Johnson, J. E., Colomb, A., Tulet, P., Molloy, S., Galbally, I. E., Volkamer, R., Mahajan, A., Halfacre, J. W., Shepson, P. B., Schmale, J., Angot, H., Blomquist, B., Shupe, M. D., Helmig, D., Gil, J., Lee, M., Coburn, S. C., Ortega, I., Chen, G., Lee, J., Aikin, K. C., Parrish, D. D., Holloway, J. S., Ryerson, T. B., Pollack, I. B., Williams, E. J., Lerner, B. M., Weinheimer, A. J., Campos, T., Flocke, F. M., Spackman, J. R., Bourgeois, I., Peischl, J., Thompson, C. R., Staebler, R. M., Aliabadi, A. A., Gong, W., Van Malderen, R., Thompson, A. M., Stauffer, R. M., Kollonige, D. E., Gómez Martin, J. C., Fujiwara, M., Read, K., Rowlinson, M., Sato, K., Kurokawa, J., Iwamoto, Y., Taketani, F., Takashima, H., Navarro-Comas, M., Panagi, M., and Schultz, M. G.: Observational ozone datasets over the global oceans and polar regions (version 2024), Earth Syst. Sci. Data, 17, 4901–4932, https://doi.org/10.5194/essd-17-4901-2025, 2025.

Klopper, D., Formenti, P., Namwoonde, A., Cazaunau, M., Chevaillier, S., Feron, A., Gaimoz, C., Hease, P., Lahmidi, F., Mirande-Bret, C., Triquet, S., Zeng, Z., and Piketh, S. J.: Chemical composition and source apportionment of atmospheric aerosols on the Namibian coast, Atmos. Chem. Phys., 20, 15811–15833, https://doi.org/10.5194/acp-20-15811-2020, 2020.

https://doi.org/10.5194/essd-2026-95
Preprint. Discussion started: 27 April 2026

Jiang, B., Xie, Z., Lam, P. K. S., He, P., Yue, F., Wang, L., et al., Spatial and temporal distribution of sea salt aerosol mass concentrations in the marine boundary layer from the Arctic to the Antarctic. J. Geophys. Res., 126, e2020JD033892. https://doi.org/10.1029/2020JD033892, 2021.

Laj, P., Bigi, A., Rose, C., Andrews, E., Lund Myhre, C., Collaud Coen, M., Lin, Y., Wiedensohler, A., Schulz, M., Ogren, J. A., Fiebig, M., Gliß, J., Mortier, A., Pandolfi, M., Petäja, T., Kim, S.-W., Aas, W., Putaud, J.-P., Mayol-Bracero, O., Keywood, M., Labrador, L., Aalto, P., Ahlberg, E., Alados Arboledas, L., Alastuey, A., Andrade, M., Artíñano, B., Ausmeel, S., Arsov, T., Asmi, E., Backman, J., Baltensperger, U., Bastian, S., Bath, O., Beukes, J. P., Brem, B. T., Bukowiecki, N., Conil, S., Couret, C., Day, D., Dayantolis, W., Degorska, A., Eleftheriadis, K., Fetfatzis, P., Favez, O., Flentje, H., Gini, M. I., Gregorič, A., Gysel-Beer, M., Hallar, A. G., Hand, J., Hoffer, A., Hueglin, C., Hooda, R. K., Hyvärinen, A., Kalapov, I., Kalivitis, N., Kasper-Giebl, A., Kim, J. E., Kouvarakis, G., Kranjc, I., Krejci, R., Kulmala, M., Labuschagne, C., Lee, H.-J., Lihavainen, H., Lin, N.-H., Löschau, G., Luoma, K., Marinoni, A., Martins Dos Santos, S., Meinhardt, F., Merkel, M., Metzger, J.-M., Mihalopoulos, N., Nguyen, N. A., Ondracek, J., Pérez, N., Perrone, M. R., Petit, J.-E., Picard, D., Pichon, J.-M., Pont, V., Prats, N., Prenni, A., Reisen, F., Romano, S., Sellegri, K., Sharma, S., Schauer, G., Sheridan, P., Sherman, J. P., Schütze, M., Schwerin, A., Sohmer, R., Sorribas, M., Steinbacher, M., Sun, J., Titos, G., Toczko, B., Tuch, T., Tulet, P., Tunved, P., Vakkari, V., Velarde, F., Velasquez, P., Villani, P., Vratolis, S., Wang, S.-H., Weinhold, K., Weller, R., Yela, M., Yus-Diez, J., Zdimal, V., Zieger, P., and Zikova, N.: A global analysis of climate-relevant aerosol properties retrieved from the network of Global Atmosphere Watch (GAW) near-surface observatories, Atmos. Meas. Tech., 13, 4353–4392, https://doi.org/10.5194/amt-13-4353-2020, 2020.

Li, R., Zhang, H., Wang, F., Ren, Y., Jia, S., Jiang, B., Jia, X., Tang, Y., and Tang, M.: Abundance and fractional solubility of phosphorus and trace metals in combustion ash and desert dust: Implications for bioavailability and reactivity, Science of The Total Environment, 816, 151495, https://doi.org/10.1016/j.scitotenv.2021.151495, 2022.

Liebenberg-Enslin, H., von Oertzen, D., and Mwananawa, N.: Dust and radon levels on the west coast of Namibia – What did we learn?, Atmos. Poll. Res., 11, 2100–2109, https://doi.org/10.1016/j.apr.2020.05.020, 2020.

Louw, D., A. Van der Plas, V. Mohrholz, N. Wasmund, T. Junker, and A. Eggert, Seasonal and interannual phytoplankton dynamics and forcing mechanisms in the northern Benguela upwelling system. J. Mar. Syst., 157, 124–134, https://doi.org/10.1016/j.jmarsys.2016.01.009, 2016.

Lu, X., Zhang, L., Zhao, Y., Jacob, D. J., Hu, Y., Hu, L., Gao, M., Liu, X., Petropavlovskikh, I., McClure-Begley, A., and Querel, R.: Surface and tropospheric ozone trends in the Southern Hemisphere since 1990: possible linkages to poleward expansion of the Hadley circulation, Science Bulletin, 64, 400-409, https://doi.org/10.1016/j.scib.2018.12.021, 2019.

Maúre, G., Pinto, I., Ndebele-Murisa, M., Muthige, M., Lennard, C., Nikulin, G., Dosio, A., and Meque, A.: The southern African climate under 1.5 °C and 2 °C of global warming as simulated by CORDEX regional climate models, Environmental Research Letters, 13, 065002, 2018.

Mass, A., Andersen, H., Cermak, J., Formenti, P., Pauli, E., and Quinting, J.: A satellite-based analysis of semi-direct effects of biomass burning aerosols on fog and low-cloud dissipation in the Namib Desert, Atmos. Chem. Phys., 25, 491–510, https://doi.org/10.5194/acp-25-491-2025, 2025.

Munday, C., Washington, R., Engelstaedter, S., Zilli, M., Harbord, S., Knight, C., Attwood, K., and Hart, N.: Southern African Climate Change: Processes, Models, and Projections, WIREs Climate Change, 16, e70025, https://doi.org/10.1002/wcc.70025, 2025.

Mupambwa, H. A., Handura, B., Howoses, V. A., Haulofu, M., Abaye, O., Miller, T., Kasarda, M., Maggs-Kölling, G., Marais, E., Gawanab, W., and Mafwila, S. K.: Exploring freshwater generation in the Namib Desert: The potential of passive fog harvesting and solar stills, Soil and Tillage Research, 254, 106718, https://doi.org/10.1016/j.still.2025.106718, 2025.

Namibia 2023 Population and housing census report, available online at https://nsa.org.na/census/wp-content/uploads/2024/10/2023-Population-and-Housing-Census-Main-Report-28-Oct-2024.pdf; last accessed 08/11/2025

Öström, E., and K. J. Noone, Vertical profiles of aerosol scattering and absorption measured in situ during the North Atlantic Aerosol Characterization Experiment (ACE-2). Tellus B, 52B, 2000.

https://doi.org/10.5194/essd-2026-95
Preprint. Discussion started: 27 April 2026

Ohde, T., and I. Dadou, Seasonal and annual variability of coastal sulphur plumes in the northern Benguela upwelling system. PLOS ONE, 13, e0192140, https://doi.org/10.1371/journal.pone.0192140, 2018.

Pandolfi, M., Alados-Arboledas, L., Alastuey, A., Andrade, M., Angelov, C., Artiñano, B., Backman, J., Baltensperger, U., Bonasoni, P., Bukowiecki, N., Collaud Coen, M., Conil, S., Coz, E., Crenn, V., Dudoitis, V., Ealo, M., Eleftheriadis, K., Favez, O., Fetfatzis, P., Fiebig, M., Flentje, H., Ginot, P., Gysel, M., Henzing, B., Hoffer, A., Holubova Smejkalova, A., Kalapov, I., Kalivitis, N., Kouvarakis, G., Kristensson, A., Kulmala, M., Lihavainen, H., Lunder, C., Luoma, K., Lyamani, H., Marinoni, A., Mihalopoulos, N., Moerman, M., Nicolas, J., O'Dowd, C., Petäjä, T., Petit, J.-E., Pichon, J. M., Prokopciuk, N., Putaud, J.-P., Rodríguez, S., Sciare, J., Sellegri, K., Swietlicki, E., Titos, G., Tuch, T., Tunved, P., Ulevicius, V., Vaishya, A., Vana, M., Virkkula, A., Vratolis, S., Weingartner, E., Wiedensohler, A., and Laj, P.: A European aerosol phenomenology – 6: scattering properties of atmospheric aerosol particles from 28 ACTRIS sites, Atmos. Chem. Phys., 18, 7877–7911, https://doi.org/10.5194/acp-18-7877-2018, 2018.

Paton-Walsh, C., Emmerson, K. M., Garland, R. M., Keywood, M., Hoelzemann, J. J., Huneeus, N., Buchholz, R. R., Humphries, R. S., Altieri, K., Schmale, J., Wilson, S. R., Labuschagne, C., Kalisa, E., Fisher, J. A., Deutscher, N. M., van Zyl, P. G., Beukes, J. P., Joubert, W., Martin, L., Mkololo, T., Barbosa, C., de Fatima Andrade, M., Schofield, R., Mallet, M. D., Harvey, M. J., Formenti, P., Piketh, S. J., and Olivares, G.: Key challenges for tropospheric chemistry in the Southern Hemisphere, Elementa: Science of the Anthropocene, 10, 10.1525/elementa.2021.00050, 2022.

Redemann, J., Wood, R., Zuidema, P., Doherty, S. J., Luna, B., LeBlanc, S. E., Diamond, M. S., Shinozuka, Y., Chang, I. Y., Ueyama, R., Pfister, L., Ryoo, J.-M., Dobracki, A. N., da Silva, A. M., Longo, K. M., Kacenelenbogen, M. S., Flynn, C. J., Pistone, K., Knox, N. M., Piketh, S. J., Haywood, J. M., Formenti, P., Mallet, M., Stier, P., Ackerman, A. S., Bauer, S. E., Fridlind, A. M., Carmichael, G. R., Saide, P. E., Ferrada, G. A., Howell, S. G., Freitag, S., Cairns, B., Holben, B. N., Knobelspiesse, K. D., Tanelli, S., L'Ecuyer, T. S., Dzambo, A. M., Sy, O. O., McFarquhar, G. M., Poellot, M. R., Gupta, S., O'Brien, J. R., Nenes, A., Kacarab, M., Wong, J. P. S., Small-Griswold, J. D., Thornhill, K. L., Noone, D., Podolske, J. R., Schmidt, K. S., Pilewskie, P., Chen, H., Cochrane, S. P., Sedlacek, A. J., Lang, T. J., Stith, E., Segal-Rozenhaimer, M., Ferrare, R. A., Burton, S. P., Hostetler, C. A., Diner, D. J., Seidel, F. C., Platnick, S. E., Myers, J. S., Meyer, K. G., Spangenberg, D. A., Maring, H., and Gao, L.: An overview of the ORACLES (ObseRvations of Aerosols above CLouds and their intEractionS) project: aerosol–cloud–radiation interactions in the southeast Atlantic basin, Atmos. Chem. Phys., 21, 1507–1563, https://doi.org/10.5194/acp-21-1507-2021, 2021.

Seinfeld, J. H., and Pandis, S. N.: Atmospheric Chemistry and Physics: From Air Pollution to Climate Change, John Wiley and Sons, Inc.,, New York, 1326 pp., 2006.

Shelley, R. U., Landing, W. M., Ussher, S. J., Planquette, H., and Sarthou, G.: Regional trends in the fractional solubility of Fe and other metals from North Atlantic aerosols (GEOTRACES cruises GA01 and GA03) following a two-stage leach, Biogeosciences, 15, 2271–2288, https://doi.org/10.5194/bg-15-2271-2018, 2018.

Shi, Z., Krom, M. D., Jickells, T. D., Bonneville, S., Carslaw, K. S., Mihalopoulos, N., Baker, A. R., and Benning, L. G.: Impacts on iron solubility in the mineral dust by processes in the source region and the atmosphere: A review, Aeolian Research, 5, 21-42, doi: 10.1016/j.aeolia.2012.03.001, 2012.

Spirig, R., Vogt, R., Larsen, J. A., Feigenwinter, C., Wicki, A., Franceschi, J., Parlow, E., Adler, B., Kalthoff, N., Cermak, J., Andersen, H., Fuchs, J., Bott, A., Hacker, M., Wagner, N., Maggs-Kölling, G., Wassenaar, T., and Seely, M.: Probing the Fog Life Cycles in the Namib Desert, Bulletin of the American Meteorological Society, 100, 2491-2507, 10.1175/bams-d-18-0142.1, 2019.

Swap, R. J., Annegarn, H. J., Suttles, J. T., King, M. D., Platnick, S., Privette, J. L., and Scholes, R. J.: Africa burning: A thematic analysis of the Southern African Regional Science Initiative (SAFARI 2000), J. Geophys. Res., 108, https://doi.org/10.1029/2003JD003747, 2003.

Tyson, P. D. and Preston-Whyte, R. A.: The Weather and Climate of Southern Africa, 2nd edn., Oxford University Press Southern Africa, Cape Town, 2014.

Valorso, R., S. Piketh, M. Cazaunau, and P. Formenti, Aerosol mass concentrations measured over coastal Namibia from 2012 to 2019. https://doi.org/10.57932/d5bcf2ef-1c1f-4f87-9945-e5ec9a948112, 2026a

https://doi.org/10.5194/essd-2026-95
Preprint. Discussion started: 27 April 2026

Valorso, R., V. Michoud, S. Piketh, M. Cazaunau, and P. Formenti, Ozone mixing ratio measured over coastal Namibia from 2012 to 2019. https://doi.org/10.57932/59ed8db1-2a18-4429-a153-fffa61cdbb41, 2026b.

Valorso, R., S. Piketh, M. Cazaunau, and P. Formenti, Aerosol scattering coefficient measured over coastal Namibia from 2015 to 2019. https://doi.org/10.57932/4d3613b6-4c49-417f-ac1d-fd825602fbfb, 2026c.

Valorso, R., S. Piketh, M. Cazaunau, and P. Formenti, Equivalent black carbon mass concentration measured over coastal Namibia from 2012 to 2019. https://doi.org/10.57932/c8c755ef-bf7a-441e-a4c6-1ee875e5f570, 2026d.

Valorso, R., S. Piketh, M. Cazaunau, and P. Formenti, Wind speed and direction measured over coastal Namibia from 2012 to 2019. https://doi.org/10.57932/99b707a5-1cba-4b61-915b-829aa742a726, 2026e.

Valorso, R., S. Piketh, M. Cazaunau, and P. Formenti, Air temperature, humidity and pressure measured over coastal Namibia from 2018 to 2019. https://doi.org/10.57932/9d344c70-2f09-4fff-a2d9-ce72f5cf1757, 2026f.

Vickery, K. J., Eckardt, F. D., and Bryant, R. G.: A sub-basin scale dust plume source frequency inventory for southern Africa, 2005–2008, Geophysical Research Letters, 40, 2013GL057321, 10.1002/grl.50968, 2013.

von Holdt, J. R. C., Eckardt, F. D., Baddock, M. C., and Wiggs, G. F. S.: Assessing Landscape Dust Emission Potential Using Combined Ground-Based Measurements and Remote Sensing Data, Journal of Geophysical Research: Earth Surface, 124, 1080-1098, https://doi.org/10.1029/2018JF004713, 2019.von Schneidemesser, E., Schauer, J. J., Hagler, G. S. W., and Bergin, M. H.: Concentrations and sources of carbonaceous aerosol in the atmosphere of Summit, Greenland, Atmospheric Environment, 43, 4155-4162, http://dx.doi.org/10.1016/j.atmosenv.2009.05.043, 2009.

Weingartner, E., Saathoff, H., Schnaiter, M., Streit, N., Bitnar, B., and Baltensperger, U.: Absorption of light by soot particles: determination of the absorption coefficient by means of aethalometers, Journal of Aerosol Science, 34, 1445-1463, 2003.

Weston, M. J., Piketh, S. J., Burnet, F., Broccardo, S., Denjean, C., Bourrianne, T., and Formenti, P.: Sensitivity analysis of an aerosol-aware microphysics scheme in Weather Research and Forecasting (WRF) during case studies of fog in Namibia, Atmos. Chem. Phys., 22, 10221–10245, https://doi.org/10.5194/acp-22-10221-2022, 2022.

Zhou, S., Salter, M., Bertram, T., Brito Azevedo, E., Reis, F., and Wang, J.: Shoreline wave breaking strongly enhances the coastal sea spray aerosol population: Climate and air quality implications, Science Advances, 11, eadw0343, doi:10.1126/sciadv.adw0343, 2025.

Zuidema, P., Redemann, J., Haywood, J., Wood, R., Piketh, S., Hipondoka, M., and Formenti, P.: Smoke and Clouds above the Southeast Atlantic: Upcoming Field Campaigns Probe Absorbing Aerosol's Impact on Climate, Bulletin of the American Meteorological Society, 97, 1131-1135, doi:10.1175/BAMS-D-15-00082.1, 2016.

Zuidema, P., A. Sedlacek, C. Flynn, S. Springston, R. Delgadillo, J. Zhang, A. Aiken and P. Muradyan: The Ascension Island boundary layer in the remote southeast Atlantic is often smoky, Geophys. Res. Lett., 45, pp. 4456-4465 doi:10.1002/2017GL076926, 2018.